Low-temperature crystal and magnetic structure of α-RuCl₃

H. B. Cao,[1,*] A. Banerjee,[1,†] J.-Q. Yan,[2,3] C. A. Bridges,[4] M. D. Lumsden,[1] D. G. Mandrus,[2,3] D. A. Tennant,[5] B. C. Chakoumakos,[1] and S. E. Nagler[1,6]

[1]*Quantum Condensed Matter Division, Oak Ridge National Laboratory, Oak Ridge, Tennessee 37831, USA*
[2]*Materials Science and Technology Division, Oak Ridge National Laboratory, Oak Ridge, Tennessee 37831, USA*
[3]*Department of Materials Science and Engineering, University of Tennessee, Knoxville, Tennessee 37996, USA*
[4]*Chemical Sciences Division, Oak Ridge National Laboratory, Oak Ridge, Tennessee 37831, USA*
[5]*Neutron Sciences Directorate, Oak Ridge National Laboratory, Oak Ridge, Tennessee 37831, USA*
[6]*Bredesen Center, University of Tennessee, Knoxville, Tennessee 37996, USA*

Single crystals of the Kitaev spin-liquid candidate α-RuCl₃ have been studied to determine the low-temperature bulk properties, the structure, and the magnetic ground state. Refinements of x-ray diffraction data show that the low-temperature crystal structure is described by space group $C2/m$ with a nearly perfect honeycomb lattice exhibiting less than 0.2% in-plane distortion. The as-grown single crystals exhibit only one sharp magnetic transition at $T_N = 7$ K. The magnetic order below this temperature exhibits a propagation vector of $k = (0,1,1/3)$, which coincides with a three-layer stacking of the $C2/m$ unit cells. Magnetic transitions at higher temperatures up to 14 K can be introduced by deformations of the crystal that result in regions in the crystal with a two-layer stacking sequence. The best-fit symmetry-allowed magnetic structure of the as-grown crystals shows that the spins lie in the ac plane, with a zigzag configuration in each honeycomb layer. The three-layer repeat out-of-plane structure can be refined as a 120° spiral order or a collinear structure with a spin direction of 35° away from the a axis. The collinear spin configuration yields a slightly better fit and also is physically preferred. The average ordered moment in either structure is less than 0.45(5) μ_B per Ru³⁺ ion.

I. INTRODUCTION

The Kitaev quantum spin liquid (QSL) is an exotic state of matter that exhibits fractionalized excitations in the form of Majorana fermions, and a realization of this physics has potential applications in the field of quantum information [1–5]. The state can be realized by considering a honeycomb lattice of $S = 1/2$ moments with either ferromagnetic or antiferromagnetic bond-directional Ising interactions, also referred to as Kitaev interactions. The necessary terms in an effective spin Hamiltonian can be realized in practice by octahedrally coordinated low-spin d^5 magnetic ions with strong spin-orbit coupling [6]. It is highly desirable to investigate the magnetic structure and excitations of these materials using neutron scattering techniques. Much attention has been paid to iridates containing honeycomb lattices with Ir⁴⁺ ions [7–15] as candidate materials for Kitaev physics. The challenges presented by the large neutron absorption cross-section and rapid decrease of the Ir magnetic form factor have limited the neutron studies of honeycomb iridates to date [13–15]. On the other hand, it is much more feasible to carry out detailed neutron scattering investigations of the binary halide α-RuCl₃, which has been proposed as an alternate candidate to realize Kitaev physics [16–22]. In this material, honeycomb layers of octahedrally coordinated low-spin Ru³⁺ ions are coupled via weak van der Waals interlayer interactions [23,24] (see Fig. 1). The single ion ground state is confirmed as effective $J = 1/2$ [18–21] and interestingly both inelastic neutron scattering [21] and Raman scattering

[17] show evidence for a continuum magnetic response that could be associated with fractionalized excitations. Neutron diffraction studies [16,20,21] have shown that the materials order in-plane with a zigzag spin structure which can arise from the Kitaev-Heisenberg model [25] as well as Kitaev-dominated models with additional more complicated interactions [26–28]. In the course of investigations of α-RuCl₃, it has become clear that sample-dependent issues have led to some confusion.

With hexagonal or honeycomb layers that are weakly coupled, it is extremely easy for the system to form stacking faults [20,29], and in fact various polytypes characterized by different stacking sequences [30] have nearly the same energy. This may be responsible for the fact that different crystal structures have been reported, including both the trigonal (T) space group $P3_1 12$ where each unit cell contains three honeycomb layers [23,24,31], and the one layer per unit cell monoclinic (M) space group $C2/m$ [32]. The low-temperature magnetic ordering transitions have similarly shown some discrepancies. Specific heat and susceptibility measurements on powders [18–21] have consistently shown a broad Néel transition at 14 K, however, many previously investigated single crystals show evidence for two separate Néel transitions at $T_N = 8$ and 14 K, and perhaps others [21], with some suggestions that these are associated with exotic physics [16,22]. A previous neutron diffraction study of single crystals with stacking faults indicated by a broad mosaicity in the direction perpendicular to the honeycomb planes [21] showed (using T nomenclature) that the 14-K transition is associated with a $(1/2, 0, 3/2)_T$ ordering wave vector corresponding to a bilayer ABAB antiferromagnetic stacking, while the 8-K transition is associated with a $(1/2, 0, 1)_T$ wave vector indicating ABC periodicity (see the transformation matrix in the note [33]). From here on we adopt the $C2/m$ symmetry
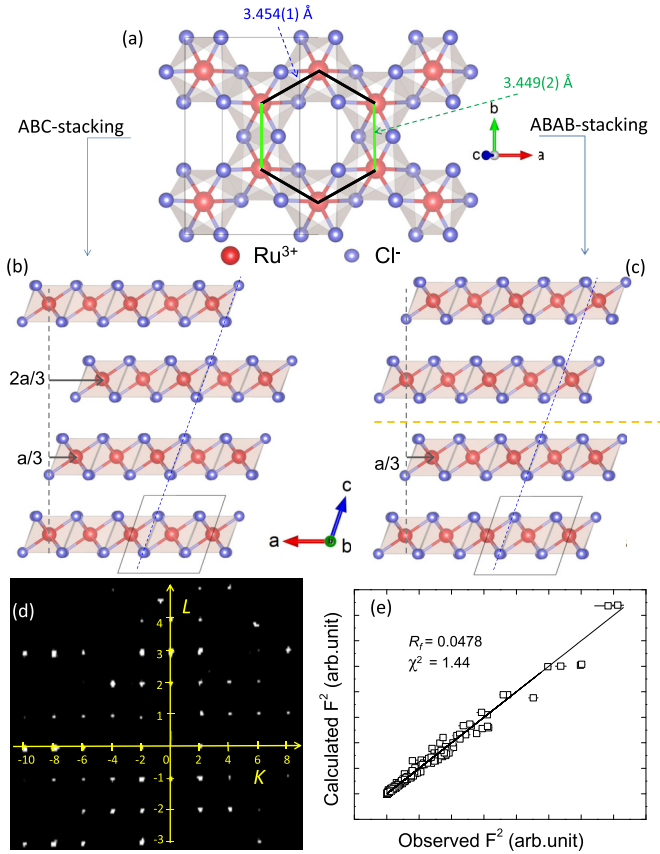
*caoh@ornl.gov
†banerjeea@ornl.gov

FIG. 1. (a) The in-plane structure of layered compound α-RuCl$_3$ viewed perpendicular to the layers along the c^* axis showing the positions of the Ru^{3+} ions (red) and Cl$^-$ ions (blue) in $C2/m$ space group symmetry. Two types of Ru^{3+}–Ru^{3+} distances are highlighted with blue [3.454(1) Å] and green [3.449(2) Å] lines (b) ABC stacking: the out-of-plane structure viewed along the b axis, showing the layered structure as well as the octahedra tilted along c. Every layer is translated by $a/3$, such that every fourth layer falls on top of the first layer when viewed along c^* (dotted line). The blue dashed line along the c axis indicates the perfect stacking for this ABC stacking. Details of the monoclinic structure are in the text as well as in Table I. (c) ABAB stacking viewed in the same orientation as that in (b), with the top two layers twinned 120° with respect to the bottom two layers. The neighboring layer is translated back and forth by $a/3$, guided by the dotted grey line (details in text). The blue dashed line along the c axis indicates the ABAB stacking is faulty stacking (orange dashed line showing the layer at which the fault occurs). (d) [0 K L] cut of the reciprocal space measured by single-crystal x-ray diffraction at 60 K. (e) The observed squared structure factors vs the calculated ones from the single-crystal x-ray data refinement.

convention, and henceforth reflections mentioned in this paper are indexed in the monoclinic lattice except for those with the label T. These structures coexist in physically separated domains in the material in different proportions in different crystals. As mentioned above, stacking faults are ubiquitous in these layered materials and in diffraction patterns show up as diffuse rods. The dependence of the magnetic wave vectors on the stacking sequence greatly complicates the solution of the crystal and magnetic structures. A recent report of structural and magnetic results on crystals that were untwinned but

exhibited significant stacking faults found that the materials were monoclinic and apparently exhibited a single, broad magnetic transition near 14 K [20]. Given that the magnetic properties can be dependent on the stacking sequence, it is crucial to study and refine the structures on single crystals of α-RuCl$_3$ with minimal stacking faults. Here we report the results of studies of such crystals. X-ray refinements of the low-temperature structure yield a monoclinic $C2/m$ space group with a symmetrical in-plane honeycomb lattice. Consistently, bulk characterization shows that the as-grown crystals exhibit a single well-defined and sharp magnetic transition at 7 K, with no signature of order apparent at 14 K. Mechanically deforming the crystals induces a magnetic transition at 14 K and the crystals subject to repeated deformations eventually exhibit only one broad transition at 14 K. The 14-K transition with its observed two-layer periodicity is likely associated with a high density of stacking faults. Neutron diffraction on a large high-quality single crystal conforms to the same monoclinic structure and only one transition at 7 K corresponding to an in-plane zigzag structure with a three-layer periodic magnetic ground state. The ordered moment is found to be small with the spin direction confined to the ac plane. Two symmetry-allowed magnetic models have been found to be consistent with the observed data: one is collinear and the other exhibits an out-of-plane spiral. The best overall refinement has been obtained with the collinear model and leads to moment directions pointing 35° away from the a axis. The possible significance of this is discussed below.

II. EXPERIMENTAL DETAILS

Commercial RuCl$_3$ powder (which has Ru^{4+} impurities in the form of partial oxides like RuOCl$_2$ and Ru$_2$OCl$_6$ and some unreacted Ru metal) [34] was purified and used to grow single crystals by vapor transport techniques at ORNL. A careful purification has been found to be critical for the growth of consistently high-quality and sizable single crystals. The as-grown crystals are shiny plates with a typical thickness of 0.5 mm but with some as large as 15 × 20 × 2 mm^3. The temperature-dependent specific heat was measured using a 9 T Quantum Design Physical Property Measurement System. For single-crystal x-ray diffraction, a 100 × 100 × 30 μm^3 as-grown untwinned crystal was carefully suspended in paratone oil and mounted on a plastic loop attached to copper pin/goniometer. The reported single-crystal x-ray diffraction data were collected with molybdenum K$_\alpha$ radiation ($\lambda = 0.710\,73$ Å) using a Rigaku XtaLAB PRO diffractometer equipped with a Dectris Pilatus 200K detector and an Oxford N-HeliX cryocooler. The raw data were examined using MAX3D [35]. Peak indexing and integration were done using 'd*trek' in the CRYSTALCLEAR package [36]. A numerical absorption correction was applied using ABSCOR [37]. The SIR-2011 in WinGX and SHELXL-2013 software packages was used for data processing and structure solution and refinement [38–40]. Crystal structure projections were made with VESTA [41]. Single-crystal neutron diffraction was performed at the HB-3A Four-Circle Diffractometer equipped with a 2D detector at the High Flux Isotope Reactor (HFIR) at ORNL. Neutron wavelengths of 1.005 and 1.546 Å were used from a bent perfect Si-331 and Si-220 monochromator

[42]. Neutrons with a short wavelength of 1.005 Å enabled a large reciprocal space coverage and were used to measure the nuclear structure. The magnetic reflections at 4.2 K and the temperature dependent magnetic intensity were measured using the longer wavelength of 1.546 Å, which also had the benefit of higher flux on the sample. The nuclear and magnetic structure refinements and representation analysis were carried out with the FULLPROF SUITE [43].

III. RESULTS

A. X-ray diffraction

More than 1300 reflections (501 unique reflections) were collected and used in the structure refinements for each temperature by XRD on a single crystal (0.003 mm^3). To assess the signal to background, we note that in a time interval producing 24 000 counts at the Bragg peak (1, 3, 1), the signal registered at a background location varied from 0–2 counts. Given this signal to noise, at all temperatures our pattern showed no diffuse scattering intensity at the $K = 3n + 1$ or $3n + 2$ ($n = $ integer) locations. At these locations, diffuse scattering rods along L are characteristic of occasional $\pm b/3$ shifts in the ab plane, and have been referred to by Johnson et al. as stacking faults of type "a" [20]. In fact, at room temperature, and also at 250 K, our diffraction pattern was free from any observable diffuse scattering. Upon cooling to 100 K, the pattern shows a faint diffuse scattering present along the L-direction in the reflections (H, K, L) with $K = 3n$. The appearance of these new diffuse scattering rods at low temperature is qualitatively similar to the observations of type "b" stacking fault scattering reported in Ref. [20]. This diffuse scattering does not appear as a continuous rod of scattering but rather as an array of weak broad peaks at the $L = n \pm 1/3$ locations, with intensity varying between 10–15 counts at the brightest spots. The upper bound for the peak intensity of diffuse scattering was 5×10^{-4} times the most intense Bragg peaks. The tiny diffuse scattering signifies that our samples have an extremely low density of stacking faults and also allows our structural refinement to use all the peaks. The $(0KL)$ slice of the diffraction data [Fig. 1(d)] show a typical slice of the XRD data. The structure solution determined a monoclinic symmetry of $C2/m$ at 60 K with lattice parameters $a = 5.981(2)$ Å, $b = 10.354(4)$ Å, $c = 6.014(2)$ Å, and $\beta = 108.800(1)°$. Table I lists the detailed structure parameters. Figure 1 shows the lattice structure in different views. Each monoclinic unit cell contains one honeycomb layer. The three Ru-Ru distances in the honeycomb are 3.454(2), 3.454(2), and 3.448(2) Å (along b), indicating a distortion of less than 0.2% [Fig. 1(a)]. Three Ru-Cl-Ru bond angles are also similar,

with values of 93.9(1)°, 93.9(1)° and 93.6(2)°. This indicates a nearly perfect honeycomb lattice, with a honeycomb distortion much lower than previously reported [20].

The data fit quality is shown in Fig. 1(e) by plotting the observed squared structure factors versus the calculated ones. With all collected reflections, the refinement yields a goodness of fit 1.44, which further indicates the diffuse scattering has a negligible effect on the refinement. In this regard, the crystals studied here are different from those reported by Johnson et al. [20] where strong diffuse scattering of types "a" and "b" had a significant effect on the structure refinement. In addition, for crystals with an edge length below 100 μm, the ratio of the crystal surface (assume the surface contains three honeycomb layers) to the crystal volume is around 10^{-4}, suggesting that the diffuse scattering observed in the present experiment may arise primarily from the crystal surface region. A total absence of the diffuse scattering in the neutron diffraction pattern in thicker crystals supports this conjecture.

B. Heat capacity

Figure 2(a) shows the heat capacity of a pristine single crystal of α-RuCl$_3$ in zero field. Over most of the temperature range, the data can be explained by a 2D Debye law as is the case with other layered materials like MoS$_2$ or graphite [44] in which the layers are loosely bound only by van der Waals forces. In such materials, several kinds of layer stacking can be expected, giving rise to a variety of distinct polytypes, due to the pseudohexagonal symmetry of the fundamental layer unit [45]. In α-RuCl$_3$, at least two types of layer stacking, ABC and ABAB type, have been proposed in the earlier report [21] based on two propagation vectors found in the ordered magnetic phases with $T_N = 8$ and 14 K, respectively. With the monoclinic lattice revealed by the single-crystal x-ray diffraction, we illustrate these two types of stacking, ABC in Fig. 1(b) and ABAB in Fig. 1(c). In a perfect RuCl$_3$ lattice, one will expect almost ideal ABC-type stacking since every layer slides by nearly $a/3$ perpendicular to the honeycomb edge from the adjacent layer. This stacking sequence can be broken, for example, by the formation of stacking faults. This can easily lead to ABAB-type order where the system prefers the $a/3$ layer shift to slide back and forth [blue guide lines along c in both Figs. 1(b) and Fig. 1(c)].

The fragility of the stacking sequence in these quasi-2D crystals is evident from the heat capacity data shown in Fig. 2(c). The as-grown crystal with minimal stacking faults shows one sharp magnetic transition at $T_N = 7$ K as illustrated by heat capacity measurements in Fig. 2(a), and confirmed with single-crystal neutron diffraction [Fig. 2(b)] measured on the magnetic Bragg peak (0, 1, 1/3) (discussed below).

TABLE I. The structure parameters of α-RuCl$_3$ measured at 60 K by single-crystal x-ray diffraction. The space group is $C2/m$ (unique axis b, cell choice 1), $a = 5.981(2)$ Å, $b = 10.354(4)$ Å, $c = 6.014(2)$ Å, $\alpha = 90°$, $\beta = 108.800(1)°$, $\gamma = 90°$. $R_f = 0.0478$, and $\chi^2 = 1.44$. U have units of Å^2.

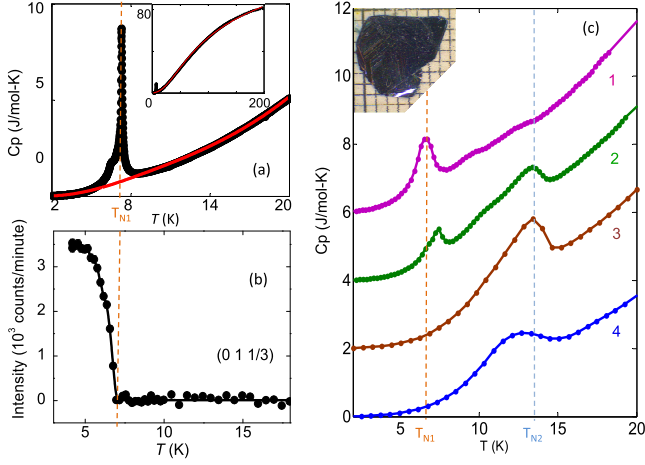| Atom	Type	Site	x	y	z	U_{equiv}	U_{11}	U_{22}	U_{33}	U_{23}	U_{13}	U_{12}
Ru1	Ru	4h	0	0.166 53(6)	1/2	0.0041(3)	0.0039(5)	0.0039(4)	0.0046(5)	0	0.0017(3)	0
Cl1	Cl	4i	0.2273(4)	0	0.7359(4)	0.0049(5)	0.0044(10)	0.0044(8)	0.0056(11)	0	0.0012(8)	0
Cl2	Cl	8j	0.2504(3)	0.173 88(12)	0.2662(3)	0.0051(4)	0.0049(7)	0.0062(7)	0.0049(8)	0.0001(5)	0.0026(6)	−0.0007(5)

FIG. 2. (a) The heat capacity of an as-grown single crystal of α-RuCl$_3$ from 2–20 K shows the low-temperature region exhibiting one sharp Néel transition at $T_{N1} = 7$ K. As determined by the neutron diffraction reported here, the in-plane magnetic order is zigzag with out of plane order corresponding to ABC stacking of the layers. The inset shows the data in the large temperature range of 2–200 K. The data excluding the 5–10 K transition region can be fit to a 2D Debye expression $C_p(T) = ANk(\frac{T}{\theta_D})^2 \int_0^{\frac{\theta_D}{T}} \frac{x^2}{e^x-1}dx$ with $\theta_D = 209(2)$ K, similar to powder [21]. (b) The thermal evolution of the intensity of the magnetic peak (0, 1, 1/3) [trigonal $(1/2,0,1)_T$] as measured at HB-3A shows a rapid fall-off near $T_{N1} = 7$ K. A crystal from the same batch as shown in (c)-inset with similar dimensions was used for the single-crystal neutron diffraction at HB-3A. (c) The heat capacity data on the same single crystal when subject to artificial deformation. The violet curve 1 represents the marginally deformed crystal and shows a rather suppressed anomaly at T_{N1} as compared to an as-grown crystal. When this crystal is manually deformed, the green curve 2 is obtained. Additional transitions, most prominently at $T_{N2} = 14$ K, appear, while the anomaly at the T_{N1} transition loses strength. When deformed further, the anomaly at T_{N1} completely vanishes leaving behind a broad anomaly T_{N2} as the only strong feature (brown curve 3). The heat-capacity of the deformed crystal resembles that of powder α-RuCl$_3$ (blue curve 4). The inset is a picture of the as-grown crystal against a grid of 1 mm^2.

If a typical crystal is not handled with enough care, the T_N loses its sharpness [Fig. 2(c)]. If this crystal is manually deformed by bending it back-and-forth a few times, new magnetic transitions appear most prominently the one at $T_N = 14$ K, while the T_N of the transition near 7 K also increases slightly to approximately 8 K, in agreement with the previous report [21]. This curve matches other reported susceptibility measurements [16,18]. Further deforming the crystal altogether obliterates the magnetic transition at 7 K (brown curve 3). The transition at 14 K is broad, and matches the magnetic transition in a powder sample (blue curve 4) with an ABAB-type magnetic order [19,21,23,24] as well as single crystals reported in Ref. [20]. Thus the material has at least two polytypes: a quasitrilayer and a quasibilayer stacking with two different Néel temperatures. Our as-grown crystals consistently show a pure quasitrilayer stacking symmetry as shown in Fig. 1(b). This quasibilayer stacking as shown in Fig. 1(c) is abundant in imperfect crystals or polycrystalline

samples. If this type of stacking fault dominates the sample, it could be responsible for the collinear ABAB-type out-of-plane antiferromagnetism observed in Refs. [20,21] below $T_N = 14$ K. Given the weak van der Waals interaction orders of magnitude lower than 1 meV [29], it takes little energy to cause stacking faults.

C. Neutron diffraction

Single-crystal neutron diffraction was performed at low-temperature on a large size crystal as shown in the inset of Fig. 2(a). While all of the reflections can be indexed in a reported trigonal lattice $P3_112$, their intensities are incompatible with a trigonal space group but conform to $C2/m$ space group consistent with the x-ray refinements. Figure 3(a) shows a scan of $(1,1,L)_T$, corresponding to $(2,0,L/3)$ in monoclinic notation [33], at two temperatures. The structure was refined including all three 120° twins [Fig. 3(b)], which propagate along the three directions perpendicular to six honeycomb edges with $a/3$ lattice shift. They define three equivalent kinds of structural domains that may exist in a larger crystal. The mosaicity along the stacking direction is 0.5° as shown in Fig. 3(c), which was limited by the instrumental resolution,
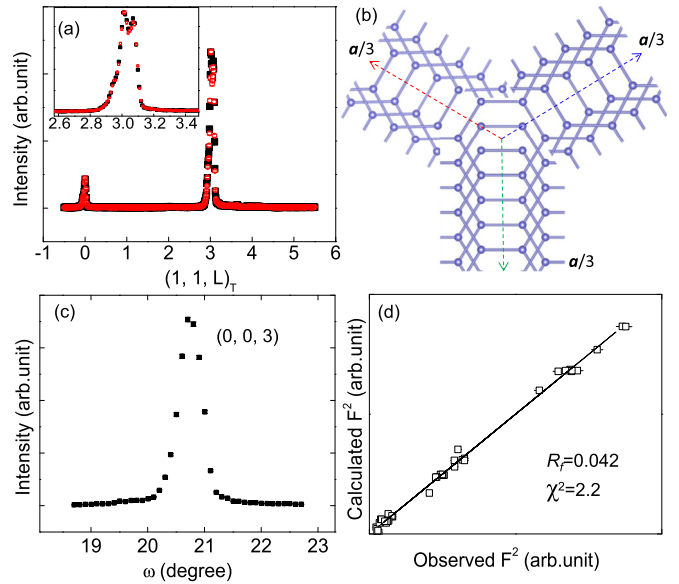

FIG. 3. (a) L scans of $(1, 1, L)_T$, $(2, 0, L/3)$ in monoclinic notation, measured by single-crystal neutron diffraction at 5 K (black solid squares) and 10 K (red open circles) at HB-3A. The reflections can be indexed in a trigonal lattice but the intensities are incompatible with a trigonal lattice symmetry. No structural change was observed from 5 to 10 K. The inset shows a close-up at $(1, 1, 3)_T$. (b) Three monoclinic structure domains form in the crystal measured by neutron diffraction. Each domain has the honeycomb layer shifted by $a/3$ along the direction perpendicular to one of honeycomb edges from one layer to the next, which yields a pseudo trigonal pattern in the neutron diffraction measurement. (c) Rocking curve scan at $(0, 0, 3)$ measured by neutron diffraction exhibits a resolution limited width of 0.5° along the stacking direction, indicating a high quality crystal with only a few stacking faults. (d) Observed squared structure factors vs the calculated ones from the neutron data refinement.

and indicates that the three 120° rotated monoclinic structure domains are well matched to each other. The reflections can be separated into three equivalent sets, and each set can be well fit with the untwinned monoclinic structure determined by x-ray diffraction. The fit quality is displayed in Fig. 3(d) by plotting the observed squared structure factors versus the calculated ones.

The two magnetic orders identified in Ref. [21], $(1/2,0,1)_T$ with $T_N = 8$ K (ABC stacking) and $(1/2,0,3/2)_T$ with $T_N = 14$ K (ABAB stacking), would appear as $(0, 1, 1/3)$ and $(0, 1, 1/2)$ type magnetic wave vectors, respectively, in the $C2/m$ space group. As expected from the heat capacity results, single-crystal neutron diffraction shows a magnetic peak at $k = (0,1,1/3)$, while no peak intensity is at $k = (0,1,1/2)$ [Fig. 4(b)], ruling out the chance of complications arising from a mixture of ABC and ABAB stacking. To obtain the correct intensities, the same scan for each peak was performed above T_N at 10 K and was used as the background. The temperature dependence of the intensity of this order was measured at the peak $(0, 1, 1/3)$ [Fig. 2(b)], which is also consistent with $T_N = 7$ K, and the intensity saturates below 5 K. The rocking curve scans measured at 4.2 K for the magnetic peaks $(0, 1, 1/3)$ and $(0, 1, 2/3)$ are shown in Figs. 4(c) and 4(d). For the magnetic structure refinement, the data were collected at 4.2 K, where the intensity has saturated, in order to obtain the correct value of the ordered moment. Data for other magnetic peaks related to the propagation vector of $k = (0,1,1/3)$ and $-k$ were collected in the same way as those two peaks shown in Figs. 4(c) and 4(d). Each of the three structural domains produces a set of magnetic peaks characterized by $k = (0,1,1/3)$. If one failed to consider the presence of the structural domains,

then the existence of three families of propagation vectors, $k_1 = \pm(0,1,1/3)$, $k_2 = \pm(1/2,1/2,1/6)$ or $(1/2, 1/2, 1/2)$, $k_3 = \pm(1/2, -1/2, -1/6)$ or $(1/2, -1/2, -1/2)$, would be inferred. Interestingly, without considering the L components, one would then obtain the same propagation vectors as reported in Na_2IrO_3, $\pm(0,1)$, $\pm(0.5,0.5)$, $\pm(0.5, -0.5)$ [10]. In both instances, these are compatible with a zigzag spin structure in each honeycomb layer. Within the resolution of the measurement, no evidence of any structural phase transition was observed across T_N between 4.2 and 10 K, consistent with the scans in Fig. 3(a).

With the propagation vector $k = (0,1,1/3)$ and the lattice symmetry $C2/m$, two magnetic symmetries are possible, Pm and Pm', yielding two well-known magnetic models, zigzag and stripy, respectively. Both the symmetries were taken into consideration for refining our magnetic models. The only models producing a reasonable fit to the data show an in-plane zigzag structure with the moments confined to the ac plane. A moment direction within that plane follows from symmetry requirements. Given the in-plane zigzag structure, a reasonable fit to the data can be obtained with the out-of-plane spin structure corresponding to either a spiral or a modulated collinear spin configuration. The spiral-zigzag model [Fig. 5(a)] has a moment size of 0.45(5) μ_B at 4.2 K with the moment direction rotating from layer to layer by $\pm 2\pi/3$. The goodness of fit (χ^2 normalized by the degrees of freedom) is $\chi^2 = 0.5$ regardless of the overall phase angle with one choice shown in Fig. 5(a). The modulated spin structures [Figs. 5(b) and 5(c)] have collinear spins but modulated sizes. The spin amplitude on the nth layer $S_n = \mu_0 \sin(\Psi \pm 2n\pi/3)$, where Ψ can be arbitrary and $\mu_0 = 0.60(5)$ μ_B at 4.2 K. Refining the spin direction shows the best fit, with $\chi^2 = 0.1$, is obtained when the spins make an angle of $\phi = \pm 35°$ away from the ab plane. The variation of χ^2 with ϕ is shown in Fig. 5(d). The implications for $\phi = +35°$ [Fig. 5(b)] and $\phi = -35°$ [Fig. 5(c)] are discussed below. The resulting spin structure, for one exemplary case $\Psi = 0$, is illustrated in Fig. 5(b). In this structure, pairs of antiferromagnetically coupled layers are separated by a single zero-ordered-moment layer. The present refinement favors the collinear model over the spiral model, but it would be useful to carry out polarization analysis to rigorously distinguish between the two.

Within the resolution of the present measurement the ordered magnetic structure exhibits a commensurate three layer periodicity. In actuality, the low temperature $C2/m$ structure exhibits a pseudo-three-layer stacking, with every fourth layer [top layer of Fig. 1(b)] displaced by $\delta a = 0.617(3)$ Å, relative to a base layer [bottom layer of Fig. 1(b)]. This corresponds to $\delta a/a = 0.028$, suggesting that a more exact stacking occurs at $3a/\delta a$, approximately 107 layers. It is natural to consider whether this could lead to a magnetic structure with an incommensurate modulation along the c axis, resulting in satellite reflections around the magnetic Bragg peaks. In the present experiment, no such peaks were detected. If such peaks exist, they may be extremely weak, or the periodicity of the incommensurate modulation may be too long (exceeding 200 layers) to be detected in the current measurement. The existing data can be explained by a purely commensurate magnetic structure.
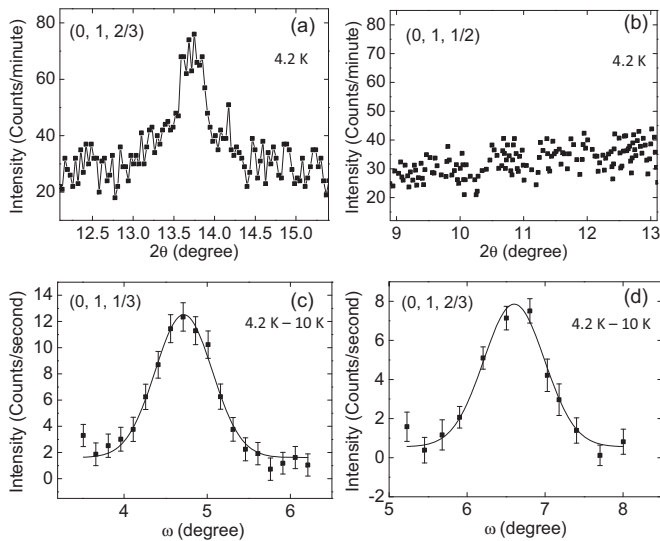

FIG. 4. Single-crystal neutron diffraction measured on α-$RuCl_3$ at 4.2 K. (a) 2θ scan at $(0, 1, 2/3)$. (b) The 2θ scan at $(0, 1, 1/2)$ does not show a peak signal, i.e., no magnetic order related to the wave vector $k = (0,1,1/2)$ exists in the measured crystal. (c) and (d) Rocking curve scans at the magnetic peaks $(0, 1, 1/3)$ and $(0, 1, 2/3)$ indicating a magnetic order with the propagation vector $k = (0,1,1/3)$. The magnetic signal was obtained by subtracting the corresponding scan above T_N at 10 K.
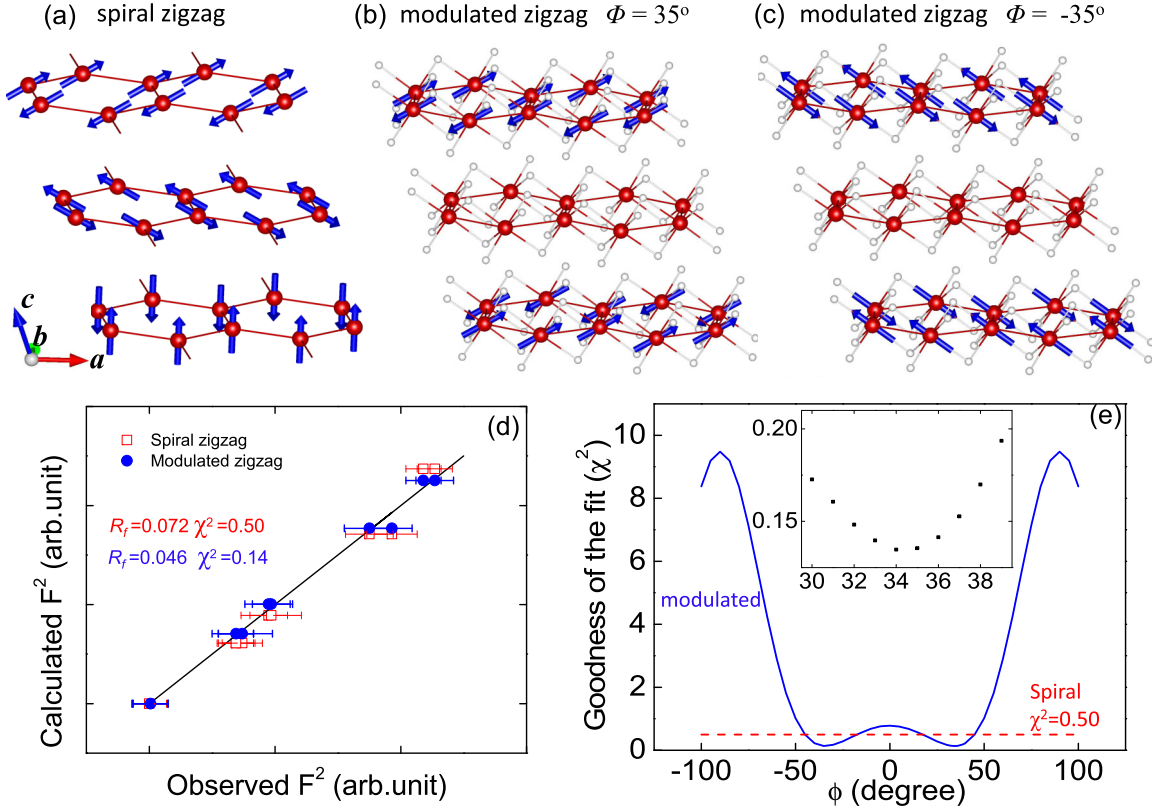
FIG. 5. Magnetic structures of α-RuCl$_3$ at 4.2 K. Large red balls represent Ru atoms. (a) Spiral zigzag magnetic structure. The spins rotate 120° from one layer to the next but the spin direction in each layer is not able to be determined by the neutron diffraction data. (b) and (c) Modulated zigzag magnetic structures showing the spins tilting $\phi = 35°$ and $-35°$ out of the ab plane. The special case with $\Psi = 0$ yields a zero-moment layer flanked by two layers with moments of magnitude 0.52 μ_B. Small white balls represent Cl atoms. (d) The observed squared magnetic structure factors vs the calculated ones for the magnetic structure refinement with the spiral (red) and modulated (blue) zigzag models. (e) The goodness of the fit χ^2 vs the spin tilting angle ϕ out of the ab plane for the spiral (red) and modulated (blue) zigzag models. The inset shows the minimum near $\phi = 35°$, the other minimum near $\phi = -35°$ has the same χ^2.

IV. DISCUSSION

The $C2/m$, $C2/c$, $P3_112$, and more generally $P3_1$ type space groups have similar in-plane arrangements of atoms but varying out-of-plane stacking sequences. These polytypes have similar configuration energies, with energy differences of the order of 1 meV per formula unit [29]. This is consistent with the well-known tendency for α-RuCl$_3$ to exhibit stacking faults [24]. It is also natural to expect that the final space group manifested can depend on the starting material purity and conditions adopted for the crystal growth. With the synthesis procedures used in the present study we have found a tendency for smaller crystals to show $C2/m$ symmetry at all temperatures, while some larger crystals form in a room temperature $P3_1$ type trigonal space group. These room-temperature trigonal crystals typically show a first-order phase transition at 155 K, resulting in a low-temperature $C2/m$ structure. Further systematic investigations are ongoing to elucidate the details of this behavior. Preliminary refinements show that the in-plane structure and the local environment of the Ru^{3+} ions remain largely unmodified. This suggests that the thermal history during the material growth and handling is important, and explains why various groups have identified different space groups for this material [23,24,29]. On the

other hand, the low-temperature structure, which determines the magnetic ground state, has always been robustly $C2/m$ in all of our crystals.

The three-dimensional magnetic ordered structure reported in various specimens of α-RuCl$_3$ consists of stacked zigzag ordered layers with a periodicity that is strongly dependent on the details of the samples. Observations to date show that powders [21] and crystals with significant diffuse scattering from stacking faults [20] show a broad transition near 14 K with alternating layers coupled antiferromagnetically. The crystals reported in this study show a single sharp transition at 7 K with a three-layer periodicity. The origin of this difference may be related to frustration of the interplane interactions as discussed below.

Previous studies of bulk properties such as the susceptibility have led to the suggestion that the interplane magnetic interactions are antiferromagnetic [16,18]. These interactions are naturally satisfied if the predominant stacking sequence is dominated by repeated monolayer or bilayer sequences, which certainly will be the case if stacking faults are plentiful as may be expected, for example, in powders, where the stacking sequence could be nearly random. The crystals measured in the present study exhibit a pseudo-three-layer stacking sequence with minimal stacking faults. Diffraction

alone cannot determine the phase angle Ψ characterizing the exact modulation in the best fit collinear structure. To gain insight, we consider the simple cases obtained for special values of Ψ when two-thirds of the layers have the same magnitude of moment. These special cases can be more generally represented by $\Psi(m) = \pi m/6$ (m is an integer) with even and odd m, respectively. For even m (e.g., $\Psi = 0$), the three consecutive planes have moments $(+0.52, 0, -0.52)$ [Fig. 5(b)]. When m is odd, the same moments are $(-0.3, 0.6, -0.3)$. The latter structure, with back-to-back ferromagnetically stacked planes, will have a higher energy if indeed the interplanar interactions are predominantly antiferromagnetic. The solution with two antiferromagnetically aligned planes and one disordered makes sense physically if one considers that the pseudo-three-layer crystal structure has a tendency to frustrate the antiferromagnetic interactions and this is the solution that relieves the frustration with minimal energy cost. This possibility remains to be tested in future measurements sensitive to local moments, for example, muon spin rotation, which might distinguish the various possible scenarios.

The refinement of the collinear structure shows that for any value of Ψ the best fit for the spin direction points approximately $35°$ away from the ab plane ($55°$ away from c^*). As discussed in Ref. [6], for edge sharing octahedra the spin-coordinate basis vectors make an angle of $\arccos(\sqrt{2/3}) = \pm 35.26°$ to the ab plane. The two directions are not physically equivalent in the monoclinic structure, but the presence of monoclinic domains makes it impossible to distinguish between them in the present experiment. With the conventions used in the paper, the choice of tilt angle $\phi = -35°$ [Fig. 5(c)] corresponds to the moment direction pointing along a Ru-Cl bond direction. This is precisely what would be expected for a leading order antiferromagnetic Kitaev interaction with a ferromagnetic Heisenberg term [12,46], and, significantly, is in agreement with the conclusions derived from inelastic neutron scattering [21]. The solution with $\phi = +35°$ [Fig. 5(b)] would be close to the situation found in Na_2IrO_3, where the moments were found to point $44.3°$ out of the ab plane [10]. Future experiments on large untwinned single crystals of $RuCl_3$ might provide a definitive experimental determination of the sign of ϕ, but the overall physical picture suggests that the moments point along the Ru-Cl ligand.

As discussed by Johnson *et al.* [20] in the $C2/m$ structure, one of the three Ru^{3+}-Ru^{3+} distances in the honeycomb lattice is inequivalent to the others. This small distortion may relieve some frustration and contribute to the formation of the low-temperature zigzag magnetic order with a small ordered moment. Our refinements show that the magnitude of this distortion is less than 0.2%. As noted previously [21], this can result in an anisotropic Kitaev term, equivalent to an additional uniaxial Ising term, in the effective spin Hamiltonian. This is one of several possible terms that can result in a spin gap within a classical spin-wave model of magnetic excitations, although such a gap is also expected to arise from quantum fluctuations, which will be strong in α-$RuCl_3$. We believe it is premature to fully attribute this gap to bond anisotropy as suggested in Ref. [20].

In a pure Kitaev model, magnetic order is absent and the $T = 0$ ground state is a QSL. In α-$RuCl_3$, a low-temperature magnetic order is believed to be formed due to subleading magnetic interactions in addition to a dominant Kitaev term. The in-plane order is always characteristic of the zigzag phase. Conversely, the precise three-dimensional magnetic order is fragile and easily altered by the formation of low-energy stacking faults [29], as proved by the drastic changes of T_N and k. From the high-temperature magnetic susceptibility, the effective paramagentic moment has been estimated as roughly $g\sqrt{[S(S+1)]} = 2.2\mu_B$ [18,19,21]. Assuming $g = 2$, a fully ordered moment projected onto one axis would yield approximately $1.4\ \mu_B$ in a neutron diffraction experiment. The measured ordered moment of $0.45\ \mu_B$ is therefore $1/3$ of the fully ordered Ru^{3+} moment. With this low ordered moment one expects that quantum spin fluctuations are dominant, and the full spectrum of magnetic excitations will not be well-described by a classical spin-wave picture. One approach might be to consider the existence of a small ordered moment as a perturbation to a QSL ground state [21].

V. CONCLUSIONS

Single crystals of α-$RuCl_3$ with minimal stacking faults are seen to consistently exhibit a low-temperature crystal structure described by the $C2/m$ space group. The magnetic structure consists of zigzag planes stacked with a three layer periodicity. The best refinement of the magnetic structure is collinear with the moment directions oriented $\pm 35°$ from the ab plane, consistent with expectations for edge-sharing octahedra. We argue that a structure with two antiferromagnetically aligned layers and one disordered layer is consistent with the refinements and is likely on physical grounds.

[1] A. Kitaev, Ann. Phys. (NY) **321**, 2 (2006).

[2] C. Nayak *et al.*, Rev. Mod. Phys. **80**, 1083 (2008).

[3] M. Yamashita *et al.*, Science **328**, 1246 (2010).

[4] T.-H. Han *et al.*, Nature **492**, 406 (2012).

[5] J. Knolle, D. L. Kovrizhin, J. T. Chalker, and R. Moessner, Phys. Rev. Lett. **112**, 207203 (2014).

[6] G. Jackeli and G. Khaliullin, Phys. Rev. Lett. **102**, 017205 (2009).

[7] Y. Singh and P. Gegenwart, Phys. Rev. B **82**, 064412 (2010).

[8] A. Biffin, R. D. Johnson, S. Choi, F. Freund, S. Manni, A. Bombardi, P. Manuel, P. Gegenwart, and R. Coldea, Phys. Rev. B **90**, 205116 (2014).

[9] J. G. Rau, E. K. Lee and H.-Y. Kee, Ann. Rev. Condens. Matter Phys. **7**, 195 (2016).

[10] S. H. Chun, J.-W. Kim, J. Kim, H. Zheng, C. C. Stoumpos, C. D. Malliakas, J. F. Mitchell, K. Mehlawat, Y. Singh, Y. Choi, T. Gog, A. Al-Zein, M. M. Sala, M. Krisch, J. Chaloupka, G. Jackeli, G. Khaliullin, and B. J. Kim, Nat. Phys. **11**, 462 (2015).

[11] Y. Singh, S. Manni, J. Reuther, T. Berlijn, R. Thomale, W. Ku, S. Trebst, and P. Gegenwart, Phys. Rev. Lett. **108**, 127203 (2012).

[12] J. Chaloupka, G. Jackeli, and G. Khaliullin, Phys. Rev. Lett. **110**, 097204 (2013).

[13] A. Biffin, R. D. Johnson, I. Kimchi, R. Morris, A. Bombardi, J. G. Analytis, A. Vishwanath, and R. Coldea, Phys. Rev. Lett. **113**, 197201 (2014).

[14] S. K. Choi, R. Coldea, A. N. Kolmogorov, T. Lancaster, I. I. Mazin, S. J. Blundell, P. G. Radaelli, Y. Singh, P. Gegenwart, K. R. Choi, S.-W. Cheong, P. J. Baker, C. Stock, and J. Taylor, Phys. Rev. Lett. **108**, 127204 (2012).

[15] F. Ye, S. Chi, H. B. Cao, B. C. Chakoumakos, J. A. Fernandez-Baca, R. Custelcean, T. F. Qi, O. B. Korneta, and G. Cao, Phys. Rev. B **85**, 180403(R) (2012).

[16] J. A. Sears, M. Songvilay, K. W. Plumb, J. P. Clancy, Y. Qiu, Y. Zhao, D. Parshall, and Y.-J. Kim, Phys. Rev. B **91**, 144420 (2015).

[17] L. J. Sandilands, Y. Tian, K. W. Plumb, Y.-J. Kim, and K. S. Burch, Phys. Rev. Lett. **114**, 147201 (2015).

[18] M. Majumder, M. Schmidt, H. Rosner, A. A. Tsirlin, H. Yasuoka, and M. Baenitz, Phys. Rev. B **91**, 180401(R) (2015).

[19] Y. Kobayashi, T. Okada, K. Asai, M. Katada, H. Sano, and F. Ambe, Inorg. Chem. **31**, 4570 (1992).

[20] R. D. Johnson, S. C. Williams, A. A. Haghighirad, J. Singleton, V. Zapf, P. Manuel, I. I. Mazin, Y. Li, H. O. Jeschke, R. Valentí, and R. Coldea, Phys. Rev. B **92**, 235119 (2015).

[21] A. Banerjee, C. A. Bridges, J.-Q. Yan, A. A. Aczel, L. Li, M. B. Stone, G. E. Granroth, M. D. Lumsden, Y. Yiu, J. Knolle, S. Bhattacharjee, D. L. Kovrizhin, R. Moessner, D. A. Tennant, D. G. Mandrus, and S. E. Nagler, Nat. Mater., doi:10.1038/nmat4604 (2016).

[22] Y. Kubota, H. Tanaka, T. Ono, Y. Narumi, and K. Kindo, Phys. Rev. B **91**, 094422 (2015).

[23] J. M. Fletcher, W. E. Gardner, E. W. Hooper, K. R. Hude, F. H. Moore, and J. L. Woodhead, Nature (London) **199**, 1089 (1963).

[24] J. M. Fletcher, W. E. Gardner, A. C. Fox, and G. Topping, J. Chem. Soc. A 1038 (1967).

[25] J. Chaloupka, G. Jackeli, and G. Khaliullin, Phys. Rev. Lett. **105**, 027204 (2010).

[26] J. G. Rau, Eric Kee-Ho Lee, and H.-Y. Kee, Phys. Rev. Lett. **112**, 077204 (2014).

[27] J. Chaloupka and G. Khaliullin, Phys. Rev. B **92**, 024413 (2015).

[28] I. Rousochatzakis, J. Reuther, R. Thomale, S. Rachel, and N. B. Perkins, Phys. Rev. X **5**, 041035 (2015).

[29] H.-S. Kim and H.-Y. Kee, arXiv:1509.04723.

[30] J. V. Smith and H. S. Yoder, Jr., Mineral. Mag. **31**, 209–235 (1956).

[31] E. V. Stroganov and K. V. Ovchinnikov, Ser. Fiz. i Khim. **12**, 152 (1957).

[32] K. Brodersen, G. Thiele, H. Ohnsorge, I. Recke, and F. Moers, J. Less-Common Met. **15**, 347 (1968).

[33] The transformation matrix $[1/2, -1/2, 0; 1/2, 1/2, 0; 1, 0, 3]$ can be used as a guide to transform the reflection indices in the monoclinic cell $C2/m$ (M) to those in the trigonal $P3_112$ (T) cell. Thus, for example, the peaks $(0,0,1)_M$, $(0,2,0)_M$, $(0,1,1/3)_M$, and $(1/2,1/2,1/6)_M$ will transform to $(0,0,3)_T$, $(-1,1,0)_T$, $(-1/2,1/2,1)_T$, and $(0,1/2,1)_T$, respectively, and vice versa.

[34] K. R. Hyde, E. W. Hooper, J. Waters, and J. M. Fletcher, J. Less-Common Met. **8**, 428 (1965).

[35] J. Britten and W. Guan, *MAX3D - A Program for the Visualization of Reciprocal Space Volumes*, IUCr Commission on Crystallographic Computing Newsletter Vol. 8 (International Union of Crystallography, Chester, England, 2007), p. 96.

[36] Rigaku, (2005) CrystalClear. Rigaku Corporation, Tokyo, Japan.

[37] T. Higashi, ABSCOR (2000). Rigaku Corporation, Tokyo, Japan.

[38] G. M. Sheldrick, Acta Crystallogr. A **64**, 112 (2008).

[39] J. Farrugia, J. Appl. Crystallogr. **45**, 849 (2012).

[40] M. C. Burla, R. Caliandro, M. Camalli, B. Carrozzini, G. L. Cascarano, C. Giacovazzo, M. Mallamo, A. Mazzone, G. Polidori, and R. Spagna, J. Appl. Crystallogr. **45**, 351 (2012).

[41] K. Momma and F. Izumi, J. Appl. Crystallogr. **41**, 653 (2008).

[42] B. C. Chakoumakos, H. B. Cao, F. Ye, A. D. Stoica, M. Popovici, M. Sundaram, W. Zhou, J. S. Hicks, G. W. Lynn, and R. A. Riedel, J. Appl. Crystallogr. **44**, 655 (2011).

[43] J. Rodriguez-Carvajal, Physica B **192**, 55 (1993).

[44] J. Krumhansl and H. Brooks, J. Chem. Phys. **21**, 1663 (1953).

[45] Y. S. Meng, G. Ceder, C. P. Grey, W.-S. Yoon, M. Jiang, J. Bréger, and Y. Shao-Horn, Chem. Mater. **17**, 2386 (2005).

[46] G. Khaliullin, Prog. Theor. Phys. Suppl. **160**, 155 (2005).